Appl. Phys. A 89, 85–89 (2007)
DOI: 10.1007/s00339-007-4207-2

Applied Physics A
Materials Science & Processing

S.F. ALVARADO[1,✉]
F. LA MATTINA[1,2]
J.G. BEDNORZ[1]

Electroluminescence in $SrTiO_3$:Cr single-crystal nonvolatile memory cells

[1] IBM Research, Zürich Research Laboratory, Säumerstr. 4, 8803 Rüschlikon, Switzerland
[2] Physics Institute, University of Zürich, Winterthurerstr. 190, 8057 Zürich, Switzerland

Received: 28 June 2007/Accepted: 29 June 2007
Published online: 17 July 2007 •

ABSTRACT Metal–insulator–metal (M–I–M) structures involving transition-metal oxides and, more recently, also perovskite oxides with resistive switching effects have attracted substantial interest in research aimed at nonvolatile memories of nanometer dimensions. Although some models are presently under discussion, it is still not clear whether the fundamental switching mechanism is an interface or a bulk property, or a combination of both. Extended defects, such as dislocation lines and changes in the oxygen vacancy concentration, are considered responsible for the conducting state, and local reduction/oxidation processes have been proposed to be responsible for the resistive switching. In addition, the role of dopants has not been discussed in depth. Here we report on an electric-field-controlled electron trapping/detrapping process involved in the resistive switching in Cr-doped $SrTiO_3$. Electroluminescence (EL) measurements reveal that during resistive switching, light emission is observed only in the switching transition from high to low conductivity. The EL spectrum is typical for Cr^{3+} in an octahedral ligand field, indicating that the switching process involves trapping/detrapping of electrons at the Cr site. With increasing conductivity of $SrTiO_3$, we observe a change from the predominant $^2E \rightarrow {}^4A_{2g}$ (R-line) to the vibronically red-shifted $^4T_2 \rightarrow {}^4A_{2g}$ transition, which points to a modification of the Cr-occupied lattice sites.

PACS 71.30.+h; 78.60.Fi; 73.40.Rw; 78.55.-m; 85.30.Tv

1 Introduction

There has been increased interest in investigating various types of nonvolatile random access memories. Different concepts are being pursued to develop storage devices with higher areal densities and lower power consumption than those of standard flash memory. One approach is to use ferroelectric polarization in a FET-like arrangement to modulate the resistance in an adjacent conducting channel [1, 2]. Simpler memory cells presently under intense investigation are based on the resistance change of a medium by means of current or voltage pulses, an effect observed in a large variety of materials. In the so-called phase-change materials, based on chalcogenide compounds [3], the mechanism for establishing the "low" and "high" resistance states is well understood, whereas for binary or ternary oxides such as Perovskites, a clear picture has not yet emerged. Current-induced bistable resistance effects or voltage-controlled negative resistance phenomena in compounds such as Nb_2O_5, TiO_2, Ta_2O_5 and NiO [4–7] and selected Perovskites exhibit strong similarities in current–voltage (I–V) characteristics from the macroscopic down to the nanometer scale [8–10], suggesting that a common scheme may be applicable.

✉ Fax: +41-1-724-8958, E-mail: alv@zurich.ibm.com

Among the models proposed to explain the physical origin of the resistance changes in these materials, one finds modified interface properties [11–13], local inhomogeneities in the conduction path [14, 15] and a phenomenological approach involving a nonpercolating domain structure [16]. While most research is done on thin-film oxide layers, a few reports on memories are based on bulk single crystals [15, 17–20]. With the availability of doped $SrTiO_3$ single crystals, which exhibit the same memory behavior as doped $SrTiO_3$ and $SrZrO_3$ films, it became possible to study the influence both lattice defects controlled by dopants and interface effects have on the performance of a model memory system. In manganites, hole doping provides a sufficiently high bulk conductivity so that both thin films [8] and single crystals [19, 20] apparently do not require any electrical formation process prior to memory operation, or this it is not discussed.

In contrast, doped and/or oxygen-deficient $SrTiO_3$ requires a dc electric stress, a so-called forming process, to drive the insulator into a conducting state, which is the prerequisite for the realization of bistable resistive memory. Extended defects such as dislocations [21] and changes in the oxygen–vacancy concentration [18, 22] are considered responsible for the conducting state achieved by forming, while local reduction/oxidation processes have been proposed as an explanation for the resistance switching mechanism [15, 23]. A possible role of controlled defects in the form of dopants has not yet been discussed in depth.

2 Experimental

Single crystals grown in air by the floating-zone method [18] were annealed at 1150 °C in Ar/H_2 5% to adjust a defined condition with respect to the Cr valence. ESR spectra taken at 80 K with a BRUKER EMX system at 9.4 GHz enable a quantitative comparison between oxidized and reduced crystals. In the oxidized sample, the absence of the Cr^{3+} signal implies that almost all Cr ions are in the tetravalent state. A direct detection of Cr^{4+} requires measurements at higher frequencies (> 34 GHz) [24, 25]. Upon reduction of Cr-doped $SrTiO_3$, a large fraction (estimated to be between 100% and 50%) of the Cr dopants change their valence to 3+ because of charge compensation due to the presence of oxygen vacancies. A reduced $SrTiO_3$ crystal with a concentration of 0.0001 mol. % of Cr was used as reference to estimate the concentration of spin centers. At this low concentration, one can assume that, upon reduction, all of the Cr atoms are converted to the 3+ valence state. Pt electrodes of 50–100 nm thickness with a typical separation of 500 μm are deposited on (100) faces of polished crystals via e-beam evaporation in either planar or capacitor geometry, producing a fully symmetric M–I–M structure. This enables optical access to the volume between the electrodes during the dc stressing and memory operation with the electric field along the main crystal axis. The luminescence experiments are performed using an optical multichannel analyzer covering a spectral range of 300–1000 nm and with a photon-counting Si avalanche photodiode for the wavelength-integrated signal in the 400–1060 nm range. All measurements are done under ambient conditions using reduced crystals. No I–M transition could be observed in the fully oxidized state or undoped reduced crystals.

In Cr-doped crystals, it was shown that the conducting state achieved by the forming is associated with a change of the Cr valence from 3+ to 4+, which suggests that Cr^{3+} can be a source of carriers for the conduction band (CB) [18]. The Cr^{3+} and Cr^{4+} impurity levels within the band gap of $SrTiO_3$ [26] will act as donor and acceptor, respectively [27–30]. In this report we present experimental evidence of an electric-field-driven electron trapping/detrapping process at the Cr site, which is involved in the resistive switching of Cr-doped $SrTiO_3$.

3 Results

3.1 *Photoexcited luminescence and electroluminescence during sample forming*

EL and photoexcited luminescence spectra, collected on unformed samples, allow us to assign the optical response to the $^2E \rightarrow {}^4A_{2g}$ transition, the typical *R*-line of Cr^{3+} in an octahedral site [31–33]. In the conducting state, however, a significantly broadened spectrum suggests that modified defect states are involved in the charge transfer, and the EL spectra indicate carrier recombination during switching from the low (LR) to the high-resistance (HR) memory state.

In pure $SrTiO_3$ the formation of oxygen vacancies during the reduction process leads to a filling of Ti 3*d* CB states and an insulator-to-metal (I–M) transition takes place when a sufficiently high electron doping is established. However, our ESR data (see Fig. 1) show that, upon reduction of Cr-doped $SrTiO_3$, a fraction of the Cr^{4+} (see methods) changes its valence to 3+, indicating that electron doping oc-

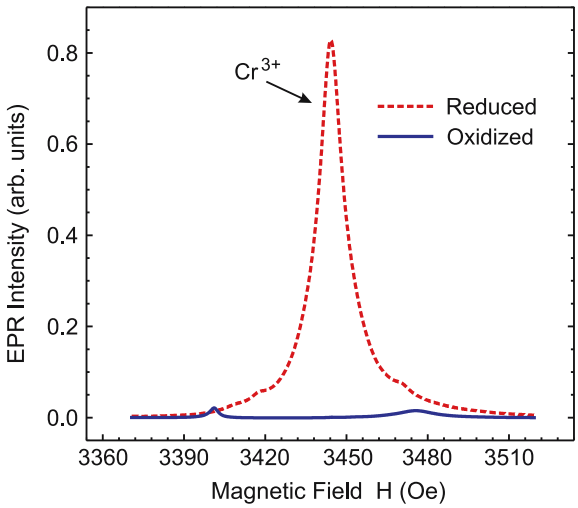

FIGURE 1 EPR Cr^{3+} *X* band signal (integrated intensity) in $SrTiO_3$ doped with 0.2% Cr. The *blue curve* is obtained in a sample oxidized 8 h at 1150 °C in an oxygen atmosphere. The *red-dotted curve* is obtained after reducing the sample by annealing for 8 h in H_2/Ar atmosphere at 1150 °C. This process produces oxygen vacancies in $SrTiO_3$, which, because of charge compensation, changes the valence of a fraction of the Cr dopant atoms from 4+ to 3+ valence

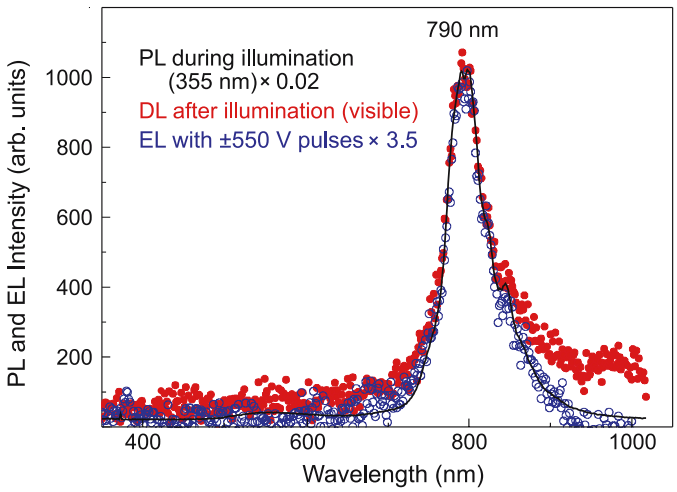

FIGURE 2 Luminescence of a $SrTiO_3$:Cr 0.2 mol % single-crystal: virgin sample at zero bias during laser (355 nm) exposure (PL) (*black line*); virgin sample in the dark during application of voltage pulses of ±550 V (EL) (*open blue circles*); spectra from a virgin samples after exposure to white light, taken with a delay of 2 s (DL) (*filled red circles*). This emission corresponds to the *R*-line, characteristic for charge-transfer processes involving Cr^{3+} in an octahedral crystal field [29, 31]. Hereby a CB electron when trapped by Cr^{4+} forms an excited Cr^{3+} state, which subsequently relaxes to the ground state via the $^2E \rightarrow {}^4A_{2g}$ transition [26, 27]

curs at the Cr-dopant sites instead [33]. The energy levels of the latter are located in the band gap of the $SrTiO_3$ host [26, 29] and, therefore, the crystals remain insulating. Because of the high initial resistance, the forming procedure has to start at a high dc voltage (up to 1 kV) in order to initiate a current flow in the nA range. As continuous carrier injection leads to an increasing current with time, the voltage is decreased in steps to keep the power at a low level to prevent irreversible damage. The final state in which stable resistive switching is established is typically reached in 5 to 10 h. This process can be accelerated by photo-excitation in the visible. It was assumed [9, 17] that the Cr^{3+} center acts as a source of carriers needed to induce the I–M transformation. Proof of an excitation of electrons involving the Cr site is provided by the spectra of the photoluminescence (PL) and EL signals, the latter excited with bias voltage pulses at relatively low currents. Both show the occurrence of a dominant line at approx. 790 nm, with a full width at half maximum of 45 nm, Fig. 2. This emission corresponds to the *R*-line, characteristic of charge-transfer processes involving Cr^{3+} in an octahedral crystal field [31, 33]. It results from the excitation of an electron from Cr^{3+} to the CB, leaving the Cr in the tetravalent state. A CB electron, when trapped by Cr^{4+}, will form an excited Cr^{3+} state, which subsequently relaxes via the $^2E \rightarrow {}^4A_{2g}$ transition to the ground state [28, 29]. Furthermore, excitation at various wavelengths (355, 633 and 780 nm) confirms that electron transfer to the CB takes place at subbandgap energies above 1.86 eV (670 nm) [28], a condition also met for irradiation in the visible. This is consistent with our ESR measurements (data not shown), which under continuous irradiation with an electric field applied show a decrease of the Cr^{3+} signal. The *R*-line emission observed both in the delayed luminescence (DL) at zero bias at the early stages of stressing and in the EL can be taken as proof of the contribution of the Cr^{3+} impurity gap states in promoting the I–M transition in $SrTiO_3$.

Near the completion of the forming process, the resistance typically decreases to the $k\Omega$ range, where the *I*–*V* loops begin to develop the hysteretic characteristics (inset of Fig. 3) required for resistive memory switching. At this stage, the system behaves metastably and has not yet developed a sufficiently large and stable asymmetry, which at low voltages should exhibit an almost ohmic behavior in the LR and a small dI/dV ratio in the HR state.

The broad EL spectrum (Fig. 3) suggests a superposition of multiple emission lines, but the *R*-line still is a dominant feature (Fig. 2), already observed before the forming process. This implies that in the conducting state the charge-transfer processes via the Cr band-gap states play a significant role in the electronic transport.

3.2 *Electroluminescence behavior of a formed memory cell*

In this particular example, we observe that by running voltage sweeps at higher currents (Fig. 4a–c), the hysteresis eventually undergoes a transition to a final stable asymmetric state. Thus, from an intermediate state (Fig. 4a), in which the memory cell remained in LR, a pronounced hysteresis can be established through sweeps at a higher compliance (80 mA), see Fig. 4b. Once a stable asymmetry is imprinted, the hystere-

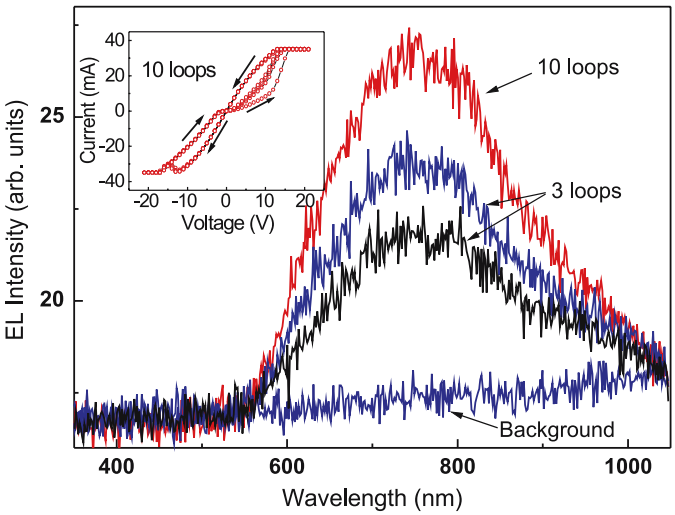

FIGURE 3 EL spectrum recorded during multiple hysteresis loops: 10 loops (*red*); three loops (*blue, black*). The spectra consist of a superposition of emission lines; one of them centered at approx. 790 nm exhibits the signature of the characteristic Cr *R*-line (Fig. 2)

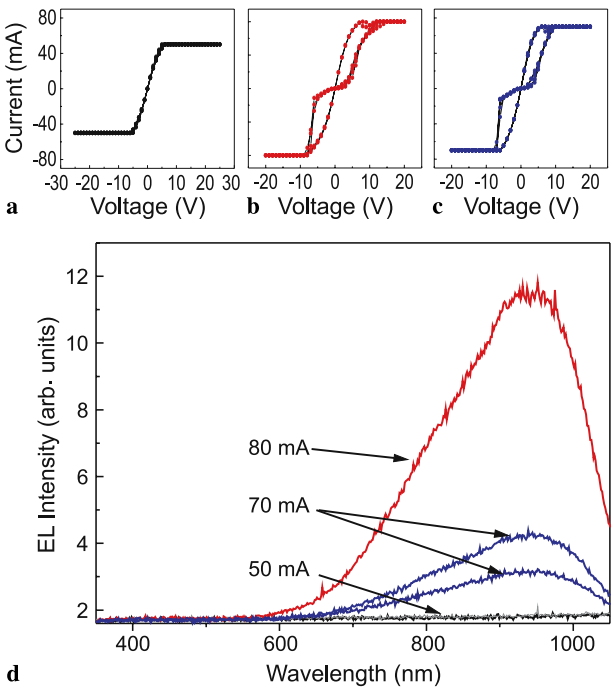

FIGURE 4 EL spectra of memory cell approaching a stable state (3 *I*–*V* loops each). (**a**) *I*–*V* loops at intermediate switching state, no switching. During these loops, no EL could be detected (background signal). (**b**) By increasing the compliance to 80 mA, a stable asymmetry is imprinted in the hysteresis. (**c**) Stable operation at compliance reduced to 70 mA. (**d**) EL spectrum obtained during stable switching loops

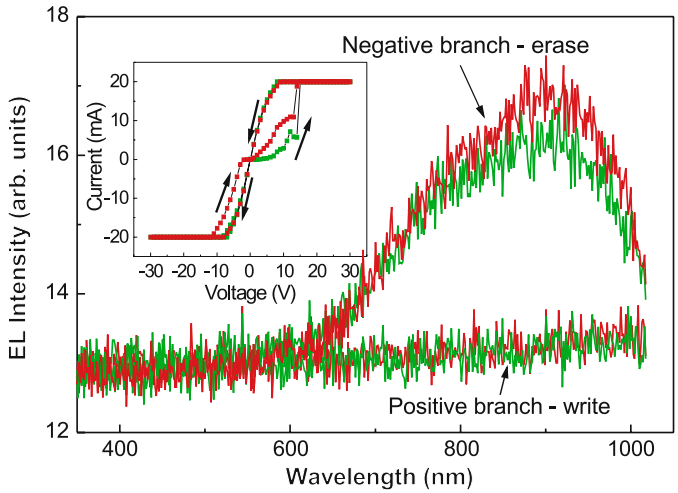

FIGURE 5 Two I–V loops with transition from a low to a high-resistance at negative polarity, and EL spectrum recorded separately for each write (positive branch) and erase (negative branch) half loop. The occurrence of the luminescence only at the erasing branch clearly indicates that this luminescence is correlated with a recombination process that decreases the number of conducting electrons

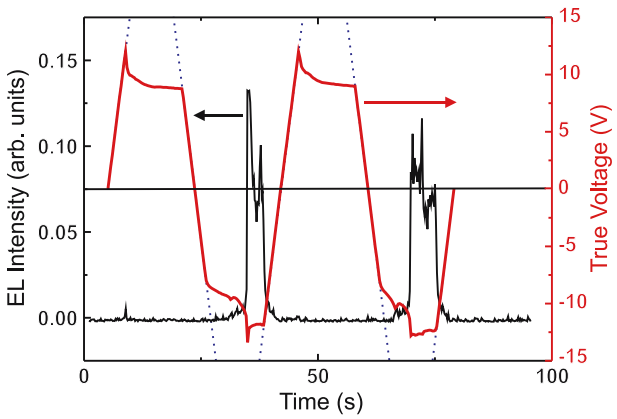

FIGURE 6 Simultaneous time-resolved luminescence (*black*) and I–V loops on a single crystal of $SrTiO_3$:Cr 0.2 mol. %. The abrupt changes of the true applied voltage curve observed in the negative branch of the hysteresis curve indicate that onset of EL coincides with an abrupt decrease in the conductance

sis is maintained by switching at lower currents (Fig. 4c).

The EL spectrum recorded during repeated voltage sweeps shows a drastic increase of intensity in the higher wavelength region, see Fig. 4, compared with Fig. 3. This is typical for a stable resistance switching, whereas no EL occurs in the intermediate state. We note that no simple relation of the EL intensity to the maximum current flowing exists. A clear EL signal with the same spectral distribution (Fig. 5) is also obtained for a memory cell operating at 20 mA. Current flow in confined regions or, in the extreme case, in filaments whose cross section can vary in different samples precludes measuring the true local power or current density. With the voltage swept in positive and negative half-loops, EL occurs in one polarity only, namely, in the negative branch of the hysteresis, where the LR to HR switching takes place. As the transition occurs while the current is in compliance, the actual true voltage applied is the relevant parameter for the detection of the switching and the correlation with the EL event. The wavelength-integrated EL signal and the true voltage measurement during a series of I–V loops are shown in Fig. 6. The abrupt changes in the V vs. t curve in the negative branch of the hysteresis indicate resistance changes that coincide with the onset of a strong EL. Apparently a threshold value either in the power density or in the applied field needs to be reached to initiate the process and maintain the EL until the voltage drops from its plateau value.

4 Discussion

A plausible explanation of the above results is that the EL arises from a dynamic process involving trapping of carriers at the Cr^{4+} centers with subsequent radiative transitions to the ground state. This is clearly the case for the $^2E \rightarrow {}^4A_{2g}$ transition. Regarding emission in the 900 to 1000-nm range, one could invoke local Joule heating due to the high currents. Luminescence spectra obtained on crystals heated up to 980 °C indicate, however, that the spectral features of the EL cannot be accounted for by black-body radiation, which leaves an electronic transition as the origin of this emission band. Such a band in this energy range has actually been observed by optical excitation in numerous compounds with Cr dopants in octahedral lattice sites [35–37] and is assigned to the $^4T_2 \rightarrow {}^4A_{2g}$ transition. This indicates that, upon forming, a change in orbital occupancy takes place from t_{2g}^3 to $t_{2g}^2 e_g^1$ [32, 38, 39]. The latter transition appears at an energy lower than the R-line because of a strong electron lattice coupling [35] with a red shift of approx. 300 nm with respect to the $^4A_{2g} \rightarrow {}^4T_2$ absorption band at 670 nm, which is comparable to that found in other oxides [35–37, 40]. Thus in our forming process, on going from the insulating to the conducting state, the emission changes from the $^2E\left(t_{2g}^3\right) \rightarrow {}^4A_{2g}\left(t_{2g}^3\right)$ (R-line) to a predominant $^4T_2\left(t_{2g}^2 e_g^1\right) \rightarrow {}^4A_{2g}\left(t_{2g}^3\right)$ transition. A plausible explanation for this shift is a nonreversible field-induced distortion of the Cr-occupied octahedral lattice site, leading to a change of the relative transition probabilities. Such a change of balance from the $^2E \rightarrow {}^4A_{2g}$ to the $^4T_2 \rightarrow {}^4A_{2g}$ emission has been observed under pressure-controlled distortion of the Cr-occupied octahedral site [40]. Evidence of an electric-field-driven modification in Cr-doped $SrTiO_3$ has been found in XAS mapping experiments, which reveal an oxygen vacancy migration into confined crystal regions [41]. This is consistent with our observed changes in EL. Therefore with progressive forming, the predominant EL shifts from the R-line, involving t_{2g} orbitals whose lobes point between the O-ligands, to EL from the $^4T_2 \rightarrow {}^4A_{2g}$ transition. The latter involves e_g orbitals represented by the $x^2 - y^2$ and z^2 $3d$ wave functions [32], which have lobes pointing towards the O-ligands. Hence both octa-

hedral distortions [27, 35, 42, 43] and oxygen vacancies will strongly affect the transition probabilities.

5 Summary

Our luminescence measurements performed on $SrTiO_3$:Cr crystals at different stages of conductivity reveal that the light emission is associated with $3d$ intrashell transitions of Cr^{3+} in an octahedral lattice site. Electrically stimulated emission can be taken as proof of dynamic processes involving trapping and subsequent radiative decay of electrons at the Cr dopant sites. With increasing conductivity, achieved during forming, the emission maximum shifts from predominant ${}^2E\left(t_{2g}^3\right) \rightarrow {}^4A_{2g}\left(t_{2g}^3\right)$ (R-line) to predominant emission from the vibronically shifted ${}^4T_2\left(t_{2g}^2 e_g^1\right) \rightarrow {}^4A_{2g}\left(t_{2g}^3\right)$ transition. The latter is associated with a change in orbital occupancy, and its energy shift can be related to a geometrical change of the oxygen octahedron, either through distortion and/or a modified oxygen–vacancy distribution. The EL in the final state, which occurs only when the memory cell is switched from the LR to the HR state, can provide an important stimulus for the refinement of theoretical models by taking controlled and defined trapping centers into account.

ACKNOWLEDGEMENTS We thank K.A. Müller, H. Keller, A. Shengelaya, G.I. Meijer, S.F. Karg and R. Macfarlane for fruitful discussions. FLM gratefully acknowledges the support by the Swiss National Science Foundation. We also thank M. Tschudy, D. Widmer, H.P. Ott and K. Wasser for competent technical assistance.

REFERENCES

1 Y. Watanabe, Appl. Phys. Lett. **66**, 1770 (1995)
2 C.H. Ahn, J.-M. Triscone, N. Archibald, M. Decroux, R.H. Hammond, T.H. Geballe, Ø. Fischer, M.R. Beasley, Science **269**, 373 (1995)
3 H.F. Hamann, M. O'Boyle, Y.C. Martin, M. Rooks, H.K. Wickramashinghe, Nature Mater. **5**, 383 (2006)
4 W.R. Hiatt, T.W. Hickmott, Appl. Phys. Lett. **6**, 106 (1965)
5 G. Argall, Solid State Electron. **11**, 535 (1968)
6 K.L. Chopra, J. Appl. Phys. **36**, 184 (1965)
7 J.C. Bruyere, B.K. Chakraverty, Appl. Phys. Lett. **16**, 40 (1970)
8 S.Q. Liu, N.J. Wu, A. Ignatiev, Appl. Phys. Lett. **76**, 2749 (2000)
9 A. Beck, J.G. Bednorz, C. Gerber, C. Rossel, D. Widmer, Appl. Phys. Lett. **77**, 139 (2000)
10 V. Szot, R. Dittmann, W. Speier, R. Waser, Phys. Stat. Solidi **1**, R86 (2007)
11 A. Baikalov, Y.Q. Wang, B. Shen, B. Lorenz, S. Tsui, Y.Y. Sun, Y.Y. Xue, C.W. Chu, Appl. Phys. Lett. **83**, 957 (2003)
12 T. Fujii, M. Kawazaki, A. Sawa, H. Akoh, Y. Kawazoe, Y. Tokura, Appl. Phys. Lett. **86**, 012 107 (2005)
13 A. Sawa, T. Fujii, M. Kawasaki, Y. Tokura, Appl. Phys. Lett. **85**, 4073 (2004)
14 C. Rossel, G.I. Meijer, D. Bremaud, J. Appl. Phys. **90**, 2892 (2001)
15 K. Szot, W. Speier, G. Bihlmeyer, R. Waser, Nature Mater. **5**, 312 (2006)
16 M.J. Rozenberg, I.H. Inoue, M.J. Sanchez, Phys. Rev. Lett. **92**, 178 302 (2004)
17 Y. Watanabe, J.G. Bednorz, A. Bietsch, C. Gerber, D. Widmer, A. Beck, S.J. Wind, Appl. Phys. Lett. **78**, 3738 (2001)
18 G.I. Meijer, U. Staub, M. Janousch, S.L. Johnson, B. Delley, T. Neisius, Phys. Rev. B **72**, 155 102 (2005)
19 A. Asamitsu, Y. Tomioka, H. Kuwahara, Y. Tokura, Nature **388**, 50 (1997)
20 Y. Tokunaga, Y. Kaneko, J.P. He, T. Arima, A. Sawa, T. Fujii, M. Kawasaki, Y. Tokura, Appl. Phys. Lett. **88**, 223 507 (2006)
21 K. Szot, W. Speier, R. Carius, U. Zastrow, W. Beyer, Phys. Rev. Lett. **88**, 75 508 (2002)
22 S. Karg, G.I. Meijer, D. Widmer, J.G. Bednorz, Appl. Phys. Lett. **89**, 072 106 (2006)
23 D. Choi, D. Lee, H. Sim, M. Chang, H. Hwang, Appl. Phys. Lett. **88**, 082 904 (2006)
24 R.H. Hoskins, B.H. Soffer, Phys. Rev. **133**, A490 (1964)
25 D.E. Budil, D.G. Park, J.M. Burlitch, R.F. Geray, R. Dieckmann, J.H. Freed, J. Chem. Phys. **101**, 3538 (1994)
26 M.O. Selme, P. Pecheur, J. Phys. C **21**, 1779 (1988)
27 K.A. Müller, Proc. 1st Int. Conf. Paramagnetic Resonance, Vol. 1 (Academic Press, New York, 1963), pp. 17–43
28 S.A. Basun U. Bianchi, V.E. Bursian, A.A. Kaplyanskii, W. Kleemann, P.A. Markovin, L.S. Sochava, V.S. Vikhnin, Ferroelectrics **183**, 255 (1996)
29 S.A. Basun, U. Bianchi, V.E. Bursian, A.A. Kaplyanskii, W. Kleemann, L.S. Sochava, V.S. Vikhnin, J. Luminesc. **66–67**, 526 (1996)
30 A.J. Silversmith, W. Lenth, K.W. Blazey, R.M. Macfarlane, J. Luminesc. **59**, 269 (1994)
31 T. Feng, Phys. Rev. B **25**, 627 (1982)
32 L.E. Orgel, J. Chem. Phys. **23**, 1004 (1955)
33 A.M. Glass, J. Chem. Phys. **50**, 1501 (1969)
34 H.D. Meierling, Phys. Stat. Solidi B **43**, 191 (1971)
35 M. Grinberg, P.I. Macfarlane, B. Hendersson, K. Holliday, Phys. Rev. B **52**, 3917 (1995)
36 G.A. Torchia, O. Martinez Matos, P. Vaveliuk, J.O. Tocho, J. Phys.: Condens. Matter **13**, 6577 (2001)
37 G.A. Torchia, O. Martinez Matos, P. Vaveliuk, J.O. Tocho, Solid State Commun. **127**, 535 (2003)
38 Y. Tanabe, S. Sugano, J. Phys. Soc. Japan. **9**, 753 (1954)
39 Y. Tanabe, S. Sugano, J. Phys. Soc. Japan. **11**, 864 (1956)
40 M. Grinberg, J. Barzowska, Y.R. Shen, K.L. Bray, B.V. Padlyak, P.P. Buchynskii, Phys. Rev. B **65**, 064 203 (2002)
41 M. Janousch, G.I. Meijer, U. Staub, B. Delley, S.F. Karg, B.P. Andreasson, Adv. Mater. (2007), in press
42 M. Grinberg, W. Jaskolski, P.I. Macfarlane, B. Hendersson, K. Holliday, J. Luminesc. **72–74**, 193 (1997)
43 K.A. Müller, K.W. Blazey, T.W. Kool, Solid State Commun. **85**, 381 (1993)